Journal of Applied Polymer Science

Structural, Mechanical, Thermal, and Electrical Properties of Carbon Black Reinforced Polyester Resin Composites

M. K. Alam,[1] M. T. Islam,[1] M. F. Mina,[1] M. A. Gafur[2]

[1]Department of Physics, Bangladesh University of Engineering and Technology, Dhaka 1000, Bangladesh

[2]Pilot Plant and Process Development Centre, Bangladesh Council of Scientific and Industrial Research, Dhaka 1205, Bangladesh

Correspondence to: M. F. Mina (E-mail: minamd.forhad@yahoo.com)

ABSTRACT: Carbon black (CB) reinforced polyester resin (PR) composites (CPC) have been fabricated from mechanical mixtures of liquid PR and CB powder having 0–50 wt% CB contents and cured with 1% of methyl ethyl ketone peroxide at room temperature under a pressure of 50 MPa. The samples have been examined by the Fourier transform infrared (FTIR) spectroscopy, X-ray diffraction (XRD) technique, scanning electron microscopy (SEM), mechanical test, micromechanical test, differential thermal analysis (DTA), and thermogravimetric analysis (TGA) and electrical test. FTIR spectra confirm the physical and chemical bond formations between CB and PR. XRD shows a very partial crystalline structure in cured PR and hexagonal structure in CB particles. SEM exhibits a clear dispersion of CB particles in PR matrix at lower loading and aggregates at higher loading. With the increase of fillers, while the tensile and flexural strengths of CPCs decrease, the Young's and tangent modulii increase by 80 and 100%, respectively. These increments are found consistent with the theoretical values. The degree of physical crosslinking between CB and PR as well as the aspect ratio of CB in CPCs are found to increase with the increase of filler. A remarkable increase in microhardness of about 61% at 50 wt% CB content is observed. The TGA represents that the thermal degradation temperature for pure PR is 373°C and that for CPC is 393°C. The dielectric constant of CPCs decreases with increasing frequency, whereas the ac- and dc- conductivities of CPC are found to increase with CB content. © 2014 Wiley Periodicals, Inc. J. Appl. Polym. Sci. **2014**, *131*, 40421.

KEYWORDS: polyester resin; carbon black; composites; mechanical property; thermal property

Received 21 September 2013; accepted 12 January 2014

DOI: 10.1002/app.40421

INTRODUCTION

In the last decades, polymers were reinforced with a variety of micron scale particles for polymer micro composites, although the recent trends to staple of modern composite technology have been changed by much smaller dimension of filler. However, these reinforced particles or fillers consist of organic and inorganic types such as silicates (mica, talc, silica, and fiber glass), metallic powders, graphite powders, carbon black (CB), etc.[1–7] Fillers have an important role in modifying various properties of polymers. Both inorganic and organic fillers are reported to improve mechanical, thermal and electrical properties of some crystalline polymers, when they are used as reinforcing agents.[1] At the particle volume fractions of the order of 15−40%, the conventional composites ordinarily get improved rigidity, but they sacrifice strength, elongation and toughness.[8]

CB is an intense black powder or bead that functions as an indispensable pigmenting and property modifying agent in a wide range of composite products. Certain unique product characteristics make CB a very valuable part of many thermoset composite formulations. These characteristics include the ability to provide polymer protection by absorbing UV energy and converting it into thermal energy, damaging its intensity when used to pigment composite parts and its ability to enhance electrical conductivity. CB is essentially elemental carbon in the form of extremely fine particles having a partially amorphous molecular structure. The primary size of the carbon black nodules are 5–100 nm which immediately cluster together to form aggregates of sizes between ~70 and 500 nm.[9] Because aggregation involves the formation of covalent bonds between primary particles and these bonds are not typically broken by physical means. Therefore, the aggregates are then subsequently combined together to form agglomerates after a few short seconds, resulting in particle sizes typically between 10 and 100 μm. The bonds formed between the agglomerates are electrostatic, and therefore cannot be broken under normal handling conditions.

In recent years, successful use of CB reinforced thermoset polymeric composites (CTPCs) has enabled new combinations of

mechanical, electrical, magnetic, optical, chemical, and surface properties, which have already been widely exploited in many industries in the automotive, electronics, packaging, aerospace, information, pharmaceuticals, biomedical, energy, sports goods, and personal care sectors. Some of the domestic and industrial appliances in which CTPCs are being used are self-regulating heating elements, current switching, fluid sensor, thermal controller, capacitors, electromagnetic interference shielding, radio frequency interference shielding, and electrostatic dissipation of charges.[6,7,10–14] Thermoset composites, including many types of unsaturated polyester, epoxy, and vinyl ester resins normally behave as insulators. General furnace processed carbon black pigments that are used as colorants for composite applications are typically resistive in nature; thus they are not suitable for conductive applications. Various research works have been carried out to develop and investigate CTPCs because of its abundant source, low density, inherent conductivity, and low cost.[4,15,16]

Most of the aforesaid works have been performed to make use of the electrical properties of the CTPCs without examining their detailed internal structure. Other applications of these composites may be offered from the comprehensive studies of their mechanical and thermal properties, which are rarely reported in the literatures.[5,17] It is an established fact that the physical property of a material is intimately related to its structure. Therefore, without knowing the structural details of a material, its physical properties cannot be improved. Considering these, the present research has been undertaken to prepare CB reinforced polyester resin composites under various processing conditions and to determine their internal structure and understand their physical properties in details in order to further develop these materials. Other points of interests of this research are to improve mechanical and thermal properties of the fabricated composites by incorporating appropriate curing agent that can enhance interfacial adhesion between resin matrix and CB. In this work, we intend to present all our observed findings that will reveal the suitability of these composites in household and industrial applications so that they can get into the mainstream of the technological proliferation.

EXPERIMENTAL

Materials and Sample Preparation

The thermosetting polymer matrix is a pre-accelerated, quick curing, anti-sagging, nonwaxed isophthalic unsaturated polyester resin (PR), supplied by Singapore Highpolymer Chemical Products (SHCP). Liquid SHCP 3155 polyester resin has clear appearance, viscosity of 1.95 Poise and cure time of 14–17 min at 30°C. The carbon black (CB) of Zhengzhou Sino Chemical, China was collected from the local market. It is a black fine powder with particle size of 10−50 μm and density of 1.7 g cm^{-3}.

PR and CB were thoroughly mixed with the weight ratios of PR : CB as 100 : 0, 99 : 1, 97 : 3, 95 : 5, 90 : 10, 80 : 20, 70 : 30, 60 : 40, 50 : 50 and hand-stirred with a glass rod for 20 min. To begin the curing processes, an amount 1% of methyl ethyl ketone peroxide (MEKP) hardener, supplied by SHCP, was poured into each mixture and further stirred for another 5 min. The final mixture was kept in a special mold arrangement at room temperature under a pressure of 50 MPa with the help of a hydraulic pressure machine for a period of 5 h until the composites become solid. Thus, CB reinforced PR composites (CPCs) were fabricated. The constant pressure was applied to eliminate the presence of possible air bubbles from the composites during the solidification process. The samples containing 0, 1, 3, 5, 10, 20, 30, 40, and 50 wt% of CB are abbreviated hereinafter as PR, 1-CPC, 3-CPC, 5-CPC, 10-CPC, 20-CPC, 30-CPC, 40-CPC, and 50-CPC, respectively. The prepared CPCs were then subjected to various property investigations.

Characterizations

Fourier-transform Infrared Spectroscopy. Fourier-transform infrared (FTIR) spectra of the samples were recorded at room temperature by using a double beam FTIR spectrophotometer (SHIMADZU, FTIR 8900 spectrophotometer, Japan) in the wave number range of 500–4000 cm^{-1}, using the standard potassium bromide (KBr) technique. For these measurements, the samples were chopped into very small pieces, mixed with KBr and then compressed in a metal holder under a load of ~8 tones to produce pellets for recording the FTIR spectrum in the transmittance (%) mode.

X-ray Diffraction Measurements. The bar samples having the same thickness were used for X-ray diffraction (XRD) measurements. Wide-angle XRD (WAXD) studies were performed by an X-ray diffractometer (model JDX-8P, JEOL, Tokyo, Japan) using the CuK_α radiation of wavelength, λ = 1.5418 Å, through a step-wise scan over the scattering angle (2θ) from 5 to 50°, with a step of 0.02°. The operating voltage and the tube current of the X-ray generator were 30 kV, 200 mA, respectively.

The degree of crystallinity (χ_c) was calculated using the equation[10]:

$$\chi_c = \frac{I_{cr}}{I_{cr}+I_{am}} \times 100 \quad (1)$$

where I_{cr} and I_{am} are the integrated intensities of crystal and amorphous parts of the samples, respectively. The crystalline thickness of the samples were calculated using the formula[18]:

$$t = \frac{k\lambda}{B\cos\theta} \quad (2)$$

where k equals 0.98, λ is the wavelength of X-ray, B is the breadth of the full-width at half maximum of the diffraction peak measured in radians and θ is the Bragg angle.

Scanning Electron Microscopy. The surface morphologies of the samples were studied by a scanning electron microscope (SEM) (Philips XL30, The Netherland) with a maximum operating voltage of 20 kV of the apparatus. The sample surfaces were coated with a thin gold layer by a sputtering machine prior to SEM measurements.

Mechanical Testing. Tensile tests of the samples were conducted by a universal testing machine (Hounsfield UTM 10KN; ASTM D-638−98) at a crosshead speed of 0.001 m min^{-1}, keeping a gauge length of 0.06 m. Tensile strength (TS) and Young's modulus (Y_m) of the samples were evaluated. Five samples of each composition were measured in the mechanical testing to obtain

the average value. The physical crosslinking density (n) between PR and CB was calculated using the theory of rubber elasticity by the following equation[4]:

$$TS = nRT\left(E_r - \frac{1}{E_r^2}\right) \quad (3)$$

where E_r is the elongation ratio, R is the gas constant equal to 8.31 J mol^{-1} K^{-1} and temperature T is 298 K. The aspect ratio (F), which is known to affect on the mechanical properties, has also been calculated using the following equation[12]:

$$F = \frac{(Y_{mc} - Y_{mr})V_{CB}}{Y_{mc}V_r} \quad (4)$$

where Y_{mc} is the modulus of virgin resin, Y_{mr} is the modulus of reinforced resin, V_{CB} is the volume fraction of carbon black, defined by $M_{CB} = [M_{CB}/(100 - M_{CB})]/\rho_{CB}$, where, M_{CB} and ρ_{CB} are the mass and density of CB, respectively, and V_r is the volume fraction of virgin resin. The value of V_r was obtained from the relation[19]:

$$V_r = \frac{\rho_s W_r}{\rho_s W_r + \rho_r W_s} \quad (5)$$

where, ρ_s is the solvent density and W_r and W_s are the weights of dry resin and absorbed solvent, respectively.

Micromechanical Testing. A software controlled Vicker's square-based diamond indenter (Shimadzu, Japan) was employed to measure the microhardness (H) from the residual impression on the sample surface after an indentation time of 6 s. Loads of 0.098, 0.245, 0.490, and 0.980 N were used to derive a load independent value of H in MPa by the following relation[20]:

$$H = K\frac{P}{d^2} \quad (6)$$

where d (m) is the length of indentation diagonal, P (mN) is the applied load, and K is a geometrical factor equal to 1.854. At least eight imprints were taken on the surface of the samples for each load, and the H was evaluated from the average value of all impressions.

Thermal Measurement. Thermal properties of the samples were simultaneously monitored by a coupled differential thermal analyzer (DTA) and thermogravimetric analyzer (TGA) [Seiko-Ex-STAR-6300, Japan]. The measurements using DTA and TGA were carried out from room temperature 25–600°C at a heating rate of 20°C min^{-1} under nitrogen gas flow of 100 mL min^{-1}. The DTA and TGA traces provide the melting and degradation temperatures of the samples as determined from exotherm versus temperature curves and the TGA runs exhibit the weight-loss of the samples with the temperature.

Electrical Measurements. Direct current (dc) conductivity (σ_{dc}) of the samples was measured by an electrometer (Keithley Electrometer 614, USA). The samples of thickness, l = 0.003−0.00035 m, were cut into a cylindrical shape of diameter, d = 0.0052 m. Both circular surfaces of the samples were coated with silver paste and then kept for 12 h before measurements. The electrometer directly displays the value of resistance of each sample. From this, the σ_{dc} value was calculated from the inverse of resistivity. Alternating current (ac) electrical measurements of the silver pasted samples were performed using a low frequency impedence analyzer (5 Hz–13 MHz, Agilent, 4192A). The values of capacitance (C) and electrical conductance (G) of each sample were simultaneously measured by the impedence analyzer. Then, real part of the dielectric constant (ε) and ac-conductivity (σ_{ac}) of the samples were evaluated from the following relations[21,22]:

$$\varepsilon' = \frac{Cl}{\varepsilon_0 A} \quad (7)$$

$$\sigma_{ac} = \frac{Gl}{A} \quad (8)$$

where $A = \pi d^2/4$, the coated-surface area of the sample.

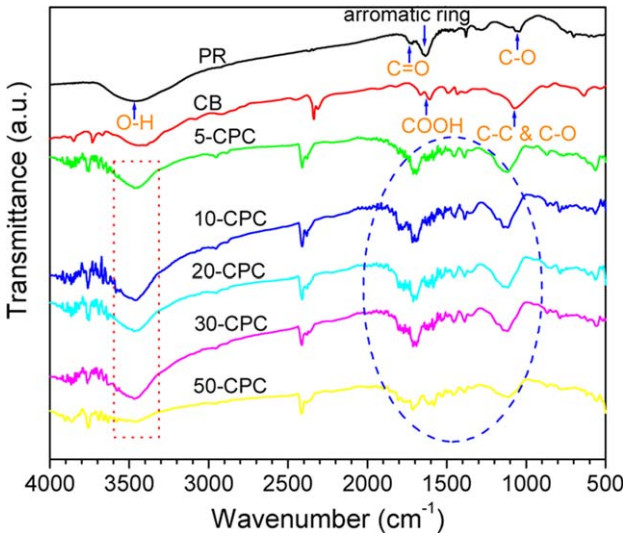

Figure 1. FTIR spectra of PR, CB, and CPC with 5, 10, 20, 30, and 50 wt% CB contents. [Color figure can be viewed in the online issue, which is available at wileyonlinelibrary.com.]

RESULTS AND DISCUSSIONS

FTIR Structural Analyses

Figure 1 illustrates the FTIR spectra of PR, CB and CPC with 5, 10, 20, 30, 50 wt% CB contents, recorded as a transmittance versus wave-number with a dotted box and encloser highlighting important variations. Among the two absorption bands appearing at 1145 and 1075 cm^{-1}, which are seen to be overlapped for the case of pure PR, the latter band is attributed to C—O stretching vibrations.[23] The peaks that appear at 1286 cm^{-1} may be assigned to CH_2 twisting, 1381 cm^{-1} to CH_3 symmetrical bending, 1640 cm^{-1} to aromatic ring stretching, 1728 cm^{-1} to C═O stretching vibrations. The bands in the range 2900–3100 cm^{-1} correspond to stretching vibrations of C—H groups, such as CH_2 and CH_3. The band at 3463 cm^{-1} may be assigned to stretching vibration of O—H groups. As can be seen from the spectra, the stretching vibration of OH group is shifted to a lower wavenumber 3458 cm^{-1} for 50 wt% CB content in the composites. From this result, it can be suggested that hydrogen bond formation may occur between PR and CB particles.

On the other hand, the spectrum of CB appears at 678 cm^{-1}, 1103 cm^{-1}, in the range 1375−1760 cm^{-1} and at 3430 cm^{-1}. CB is generally a graphite powder, which may contain

paracrystalline structure. Generally, CBs may have chemisorbed oxygen complexes (i.e., carboxylic, quinonic, lactonic, phenolic groups, and others) on their surfaces to varying degrees depending on the conditions of manufacture. The observed spectrum of CB is, in general, similar to the example found in the literature.[24] The FTIR results here seemingly show a well-defined presence of functional groups on the surface of CB, corresponding to structures featuring carbonyl and carboxyl groups. The breadth of the carbonyl absorption band envelope (at 1735-1700 cm^{-1}) reflects a mixture of different groups attached to a polyaromatic structure (anhydrides, lactones at 1735 cm^{-1}, aldehydes (at 1700 cm^{-1}). Because of the acidic nature of carbon blacks, some of these groups may be carboxylic acids (at 1700-1720 cm^{-1}). The presence of phenolic (C—O stretch at 1224 cm^{-1}) and carbonylic compounds in CB can be located between 1150 and 1300 cm^{-1}.[24] It is also evident that the presence of water in the carbon black and KBr give rise to a broad OH stretching band.

After loading of CB in PR matrix, changes in chemical textures occur, leading to the shifts of wavenumber toward higher frequencies in all the spectra of CPCs. A wide band 1154 cm^{-1} may be the representative of chemical crosslinking between CB and PR. An intense peak is observed at 1730 cm^{-1}, which may indicate the esterification (C—O—C) of PR with CB particles. Two peaks appearing at 1486 and 1419 cm^{-1} may denote the bond formations between CB and PR. Weak bands at 1599, 1580, and 1493 cm^{-1} observed in the spectrum of PR can be assigned to aromatic ring. Moreover, the band at 2350 cm^{-1} may be attributed to the graphite bond. The peak from this bond is shifted towards higher wavenumber in the composites, thereby representing an interaction between CB and PR molecules. Possible reaction mechanisms among PR-PR molecules and PR-CB are given in Figure 2 (Scheme-1 and 2). The number of C—O—C bonds (Scheme-1) between PR-PR molecules without presence of CB or with low content of CB in CPCs is assumed to be comparatively higher than that (Scheme-2) between PR molecules and CB. This assumption on esteric bond formation is made on the basis of more reaction sites in PR molecules than in CB particles. The formation of hydrogen bond is also shown.

XRD Structural Analysis

Figure 3 shows the XRD profiles of PR, CB, 3-CPC, 30-CPC, and 50-CPC. The XRD profiles reveal that polyester resin shows a broad peak at 20.29° that corresponds to its partial crystalline and high amorphous natures, because the shape of the peak is not as diffused as that usually shown by a completely amorphous matter. The average lattice spacing estimated from the peak is about 4.47 Å. When 3 wt% CB is introduced in PR, the peak width slightly decreases and a new sharp peak appears at $2\theta = 26.26°$, without any considerable shift in the PR-peak position. Increased CB content decreases the PR-peak width. This result indicates a change in the average thickness of the PR crystallites. Moreover, increasing CB content not only increases the intensity of the sharp peak but also increases its scattering angle to $2\theta = 26.40°$. These results suggest more crystalline packing in CB in the presence of PR. Besides, other sharp peaks for CB also appear in the profiles of 50-CPC at $2\theta = 28.57°$,

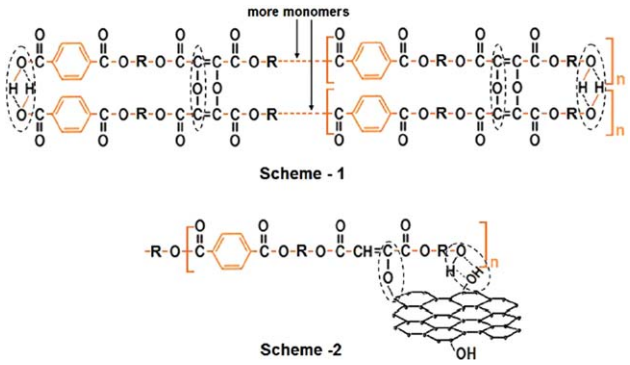

Figure 2. Possible bonding between PR-PR molecules (Scheme-1) and PR-CB (Scheme-2) [Color figure can be viewed in the online issue, which is available at wileyonlinelibrary.com.]

39.84°, 43.31°, 54.24°, and 77.60°, which are indexed as (002), (100), (101), (004), and (110) planes, as also reported elsewhere.[25] The carbon black exhibits similar structure as that shown by the graphite crystallite, which is generally of the hexagonal form.[23] On the other hand, due to the increase in CB contents the intensity of the diffused peak of PR is reduced at the cost of increasing intensities of CB-peaks, while the width of the PR-peak is greatly reduced. These results may indicate that the thickness of the ordered molecules in the pure PR decreases in the particulate reinforced PR. In other words, the size of PR crystallites increases due to particle loading.

The degree of crystallinity, χ_c, for virgin PR, CB, 3-CPC, 30-CPC and 50-CPC has been calculated, as shown in Figure 4. It is seen that the χ_c value increases with increasing CB content in the composites. This indicates that the CB particles react with resin matrix, leading to an increase in the interfacial adhesion among filler and matrix which is consistent with the previously reported result for CB reinforced epoxy/resin.[4] The average crystalline thickness, *t*, estimated for various samples are also shown in Figure 3, replacing a slight decrease in the size of the PR crystallites.

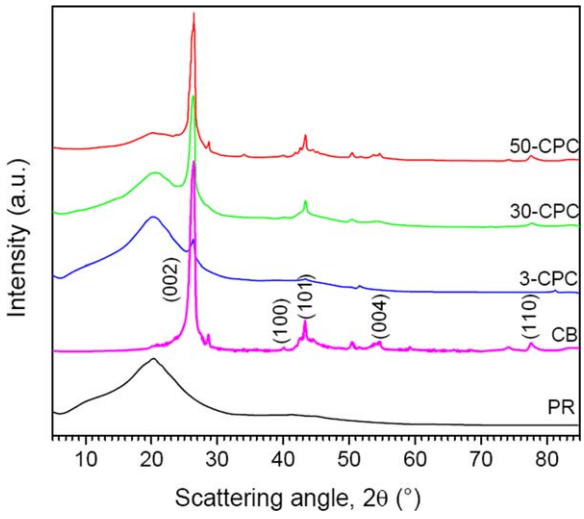

Figure 3. WAXD profiles of PR, CB, and CPC with 3, 30, and 50 wt% CB content. [Color figure can be viewed in the online issue, which is available at wileyonlinelibrary.com.]

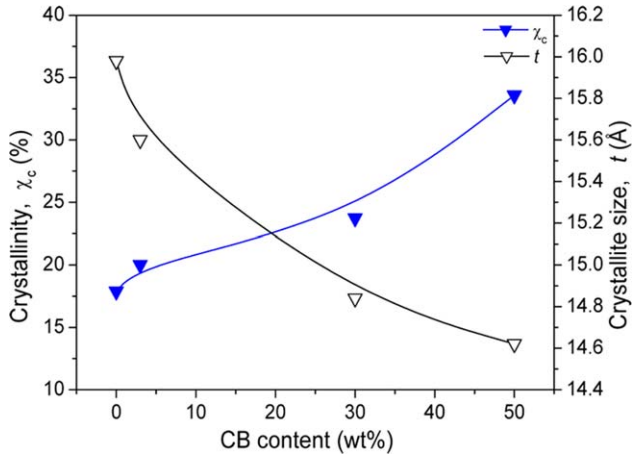

Figure 4. The changes in crystallinity, χ_c, and crystallite size, t, of the samples at various concentrations of CB. [Color figure can be viewed in the online issue, which is available at wileyonlinelibrary.com.]

Mechanical Properties

The average TS and Y_m evaluated from mechanical tests for various samples are shown in Figure 5. The TS value for the pure PR sample is 46.6 MPa, while it gradually falls down to a value of 23.5 MPa for composite with 50 wt% CB content. On the other hand, contrary to the decrease in the TS value, the Y_m is found to increase with the increase of CB contents. The minimum value of Y_m observed for the pure PR sample is 0.97 GPa and the maximum Y_m value obtained for composite sample with 50 wt% CB is 1.75 GPa. Therefore, the highest increase in the tensile modulus obtained here is 80 %.

The lower tensile strength of the composites at increasing volume fraction could be due to a number of reasons, such as less crosslinking among PR molecules, weak interfacial bonding at CB and PR matrix interfaces, agglomeration of carbon black particles, process-related defects such as porosity and so on. In case of pure PR, the crosslinking among its molecules mainly

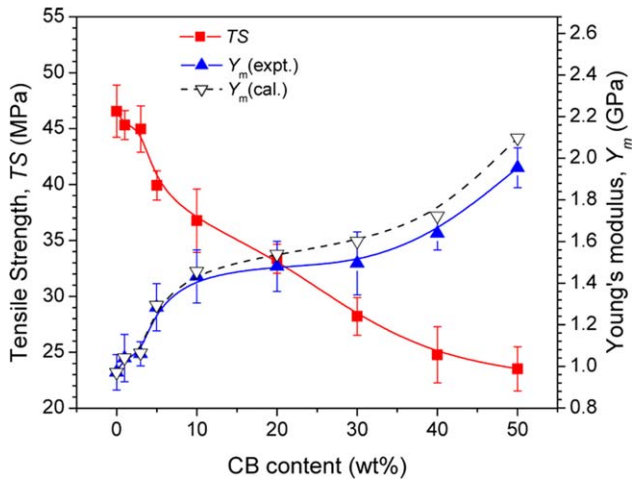

Figure 5. The variations in tensile strength and Young's modulus of the samples at various contents of CB. The solid and dotted lines indicate observed and calculated data for Y_m. [Color figure can be viewed in the online issue, which is available at wileyonlinelibrary.com.]

occur by the curing agent MEKP. If CB is present in PR, it inhibits the crosslinking among the host molecules, although a less possibility of the linkage between CB and PR may not be ignored. Thus, the TS value decreases in CPC with increasing CB loading. It is noteworthy that the tensile strength of a material is the maximum stress exhibited by it under deformation. During the deformation processes, the position and movement of CB aggregates, PR molecules and developed pores during fabrication inside the material may lessen the resulting interaction among PR-PR, CB-CB, and PR-CB molecules. This lessening of interaction is assumed to reduce the TS values of the composites with increasing CB content. Moreover, the adsorption of the carbon filler limited wettability in the polyester matrix phase may result in poor interface adhesion of carbon black particles to the polyester resin matrix and causes inefficient stress transfer between the particle–matrix interface as long as the load is applied.

A number of researchers have documented TS variations with changing filler contents in various polymers, where they reported that TS decreases with the increase of filler content. Some of them explained this fact using the following Nielson model[26]:

$$\frac{TS_C}{TS_P} = (1-\varphi^{\frac{2}{3}})A_Q \tag{9}$$

where TS_C and TS_P denote the tensile strength of the composite and the polymer matrix, respectively; φ represents the weight fraction of the filler; A_Q accounts for the adhesion quality between polymer–filler interface. According to the above formula, if a discontinuity in stress transfer to polymer–filler interface occurs, then the value of A_Q decreases. Hence, a decrease in the tensile strength of the composites with the addition of filler content is reasonable, because the TS_C value decreases as according to eq. (9). Thus, the Neilson model is better suitable to explain well the observed TS decrease with the increase of filler content.

On the other hand, if the gradual increment in Y_m with the increase of CB content is supposed to take place by the increased interactions between PR-PR, PR-CB, and CB-CB molecules, a contradiction on the TS-decrease due to weak interactions, as mentioned above, can be severely raised. To surmount this apparent anomaly of Y_m-increase and TS-decrease with the increase of filler content, it is necessary to differentiate the two physical parameters Y_m and TS and how they are measured. The Y_m is principally associated to the interactions among the molecules, whereas TS is associated to both the interactions among the molecules and the deformation processes involved in the material. As mentioned above that there exists three categories of molecule–molecule interactions of which at least one is predominant for the gradual increase in Y_m. Because Y_m increases due to the increase in CB content, it is, therefore, not illogical to consider that the Y_m gradually increases probably because of the increase of filler–filler or CB–CB interactions. Besides, the change in Y_m also relies on the dispersion of CB in PR matrix. Usually, due to its large surface area, CBs have a greater contact either with PR or with themselves. If the CB particles find a good dispersion in the PR matrix, the well

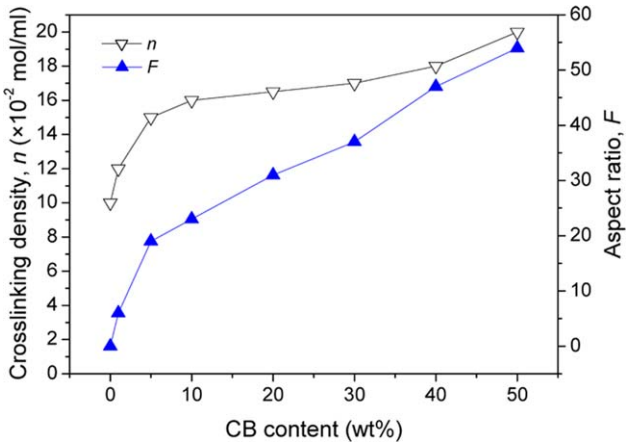

Figure 6. The changes in crosslinking density and aspect ratio with respect to particle contents. [Color figure can be viewed in the online issue, which is available at wileyonlinelibrary.com.]

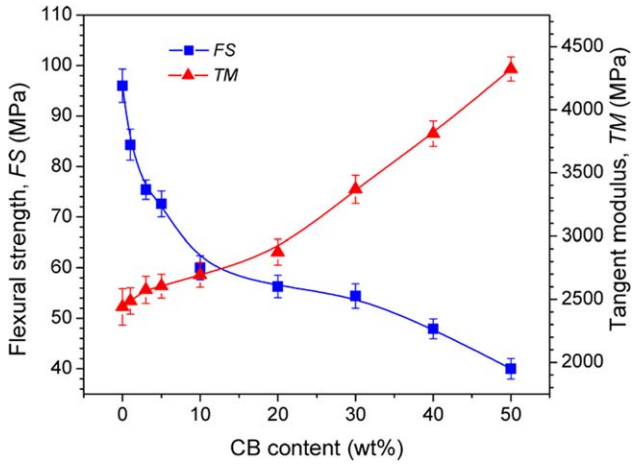

Figure 8. The dependence of flexural strength and tangent modulus of the samples at various contents of CB. [Color figure can be viewed in the online issue, which is available at wileyonlinelibrary.com.]

dispersed particles may get larger surface contacts, which essentially play roles to increase the tensile modulus of the material. A theoretical model has been given by Guth–Smallwood to predict the theoretical modulus (Y_{th}) by a widely used equation in polymer-filler composites[12]:

$$Y_{th} = Y_{mr}(1 + 2.5V_{CB} + 14.2V_{CB}^2) \quad (10)$$

The calculated Y_{th} values for CPCs plotted in Figure 5 (dotted line), gives a reasonable good fit. Thus, the volume fraction or the surface contact shows a greater influence on increasing the Y_m value of the composites. However, a small deviation between Y_{th} and Y_m due to high CB-loading may be attributed to the formation of aggregates and voids in the composites. Thus it is notable that CB particles influence largely on the Y_m value since they make physical crosslinking or network structure both with resin molecules and themselves.

To further understand the effect of CB particles on the network structure, the cross linking density (n) and the aspect ratio (F) are estimated. The dependencies of n and F verses weight fraction of CB are shown in Figure 6. It is found that n increases with increasing CB loadings in the resin composites. This likely refers to the increase in intermolecular forces among resin chains and CB particles. A scheme of probable physical crosslinking between CB particles and resin molecules is drawn by means of the rubber elasticity theory and presented in Figure 7, where CB is shown to exhibit aggregates form due to filler–filler interactions. As a result, the aspect ratio of the filler may change. Thus, the F-increase with increasing CB content in the composites can be explained by interfacial interactions among CB particles. For the development of network structure in CPC, the modulus increases.

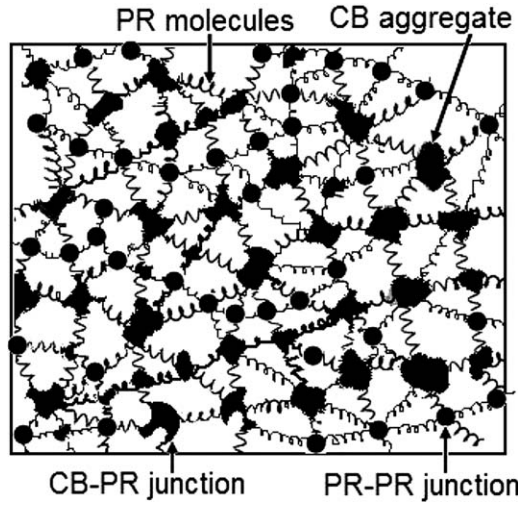

Figure 7. A scheme showing chemical and physical crosslinking among PR molecules along with CB and PR.

Figure 8 shows the flexural strength (FS) and tangent modulus (TM) verses CB plots. The trends of TM-increase and FS-decrease are similar to those of Y_m and TS, respectively. Thus, similar arguments as that set for TS and Y_m changes can also be given for the changes of FS and TM.

Micromechanical Properties

Figure 9 shows the change in microhardness with increasing load, P, for pure PR and various contents of CB loaded composites. The microhardness apparently remains unchanged with the increase of the load up to 3000 mN. Nevertheless, a slight variation of hardness with load is observable. To remove this variation or to observe the load independent hardness for different concentrations of CB, d^2 versus P for pure PR, 30 and 50 wt% of CB loaded PR composites are shown in the Figure 10. The microhardness gradually increases with the increase of CB content and becomes the maximum at 50 wt% CB content, as shown in Figure 11. The microhardness for pure PR is 140 MPa and for 50 wt% CB loaded composite is 225 MPa. Therefore, the maximum increase in H values is 61%. The microhardness provides information of micromechanical property of a material within a micro region. The observed enhancement in H can be attributed to the increased CB content, as also affected by their surface area, as well as the increase in the crystallinity of the resulting material.

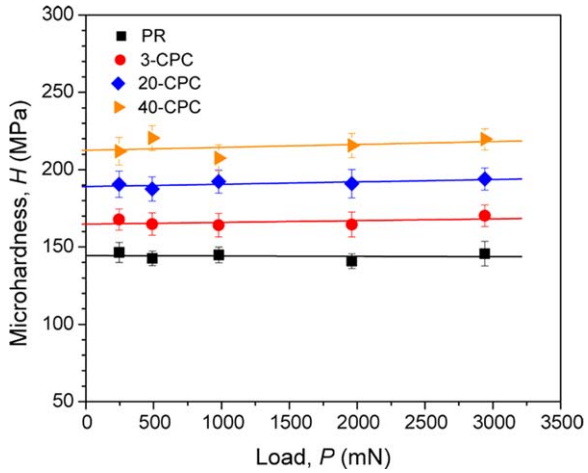

Figure 9. Microhardness as a function of load plots for PR and CPC with 3, 20, and 40 wt% CB content. [Color figure can be viewed in the online issue, which is available at wileyonlinelibrary.com.]

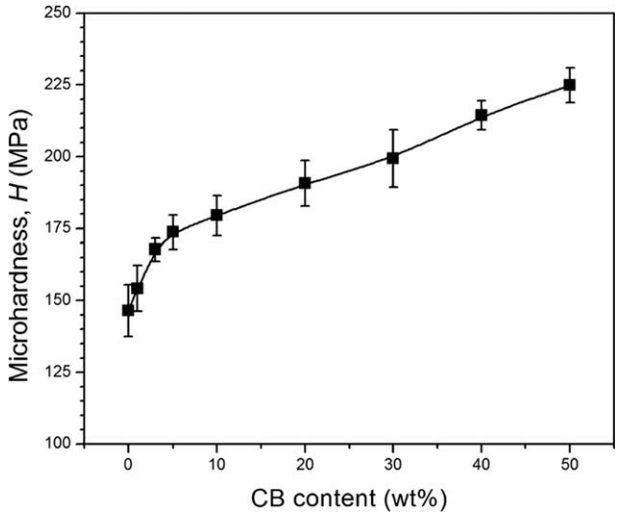

Figure 11. The change in microhardness with CB contents.

The hardness of a polymer or polymeric composites can be described in terms of its crystalline hardness H_c, and amorphous hardness H_a, according to the additivity law[27]:

$$H = H_c\chi_c - H_a(1-\chi_c) \quad (11)$$

Moreover, the H_c of a polymeric material related to the crystal thickness t and surface energy parameter b through the following expression[28]:

$$H_c = \frac{H_c^{\infty}}{1+b/t} \quad (12)$$

where, H_c^{∞} is the hardness of an infinitely thick crystal and $b = 2\sigma_e/\Delta h$, in which σ_e is the free surface energy and Δh is the energy for the plastic deformation of the crystal of a material. Thus, it is clear that σ_e and b values influence on the hardness value of a material. In case of CPC, the value of σ_e may decline after blending CB into PR, because particle incorporation makes the surface of the polymer rougher than that of pure PR.

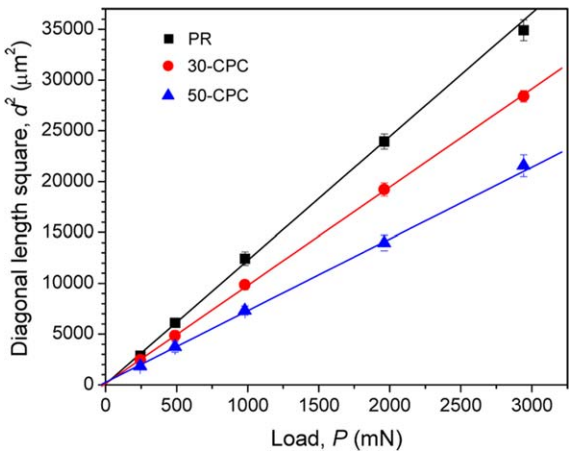

Figure 10. Square of indentation diagonal versus load plots for PR and CPC with 3 and 50 wt% CB content. [Color figure can be viewed in the online issue, which is available at wileyonlinelibrary.com.]

On the other hand, a slight decrease in the crystalline thickness or t values is observed from XRD studies. As a result, the term b/t in the denominator decreases sufficiently, thereby causing an increase in hardness as according to eq. (12). Moreover, CB particle is comparatively harder than the polymer. Therefore, the increase in hardness with the increase in CB particles is also plausible. A detailed review on the strength of particulate–polymer composites has been presented with many phenomenological and semiempirical models, relying on the parameters of particle size, interface adhesion and particle loading,[29] where it is claimed that a few weight per cent particulates with high particle size can largely improve micromechanical properties. The observed mechanical and micromechanical properties of the resulting composites can be useable in any suitable applications like indoor and outdoor panels, structures, bodies, furniture and commodities.

Surface Morphology

Figure 12 represents the SEM micrographs of virgin PR, and CPC with 5, 10, and 40 wt% CB content. A little roughness is observed in the micrograph of virgin PR, because some striations are found on the surface. On the other hand, the striations somewhat reduce after inclusion of CB in PR. Roughness increases in the surface of 5-CPC and 10-CPC. These can support the b-decrease and hardness increase that is consistent with eq. (12). The dispersion of CB in these two samples is apparently good. In contrast, random distribution and clusters of CB are found in the images of 40-CPC, whose surface structure is found to be relatively smooth. It seems that in the images of CPC with higher content of CB (40 wt%), CB channels or pathways are formed. Clusters or agglomerations are formed due to the particle–particle interactions of CB. Slight voids are also developed at 5 and 10 wt% CB loaded PR composites. Such voids are almost removed when particle concentration is greater than 30 wt%. The random distributions of CB in CPC can make physical crosslinking with PR, as has been shown in a scheme (Figure 7). The crosslinking among PR molecules are also shown. The surface morphology of CPC apparently supports the proposed crosslinking of CB and PR.

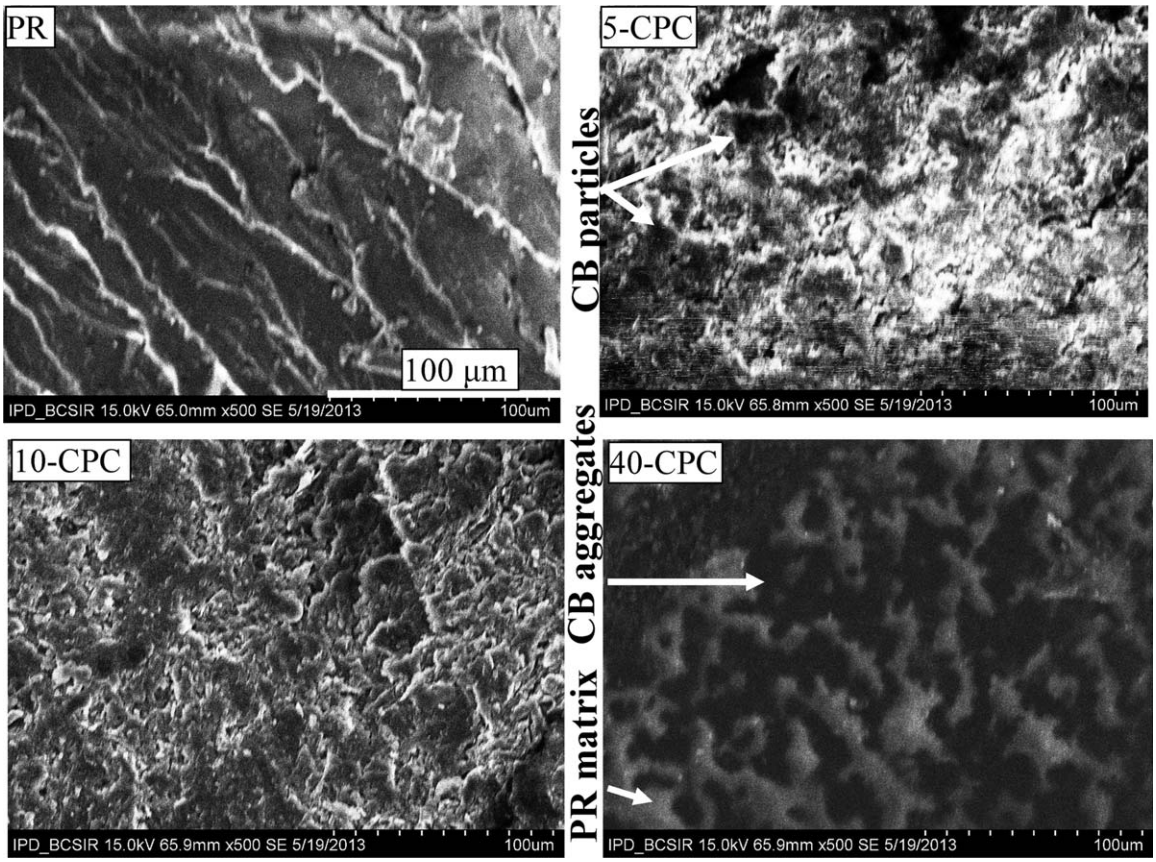

Figure 12. SEM micrographs of PR and CPC with 5, 10, and 40 wt% CB contents.

Thermal Properties

DTA curves of the samples are shown in the Figure 13. All thermograms indicate a broad endothermic peak at around 400°C with similar pattern except the pure resin. This temperature is probably the degradation temperature (T_d) of PR, observed by DTA. The pure PR also shows an exothermic peak after this temperature. Table I represents the T_d values for different samples, showing a slight increase with the increase in particle loading.

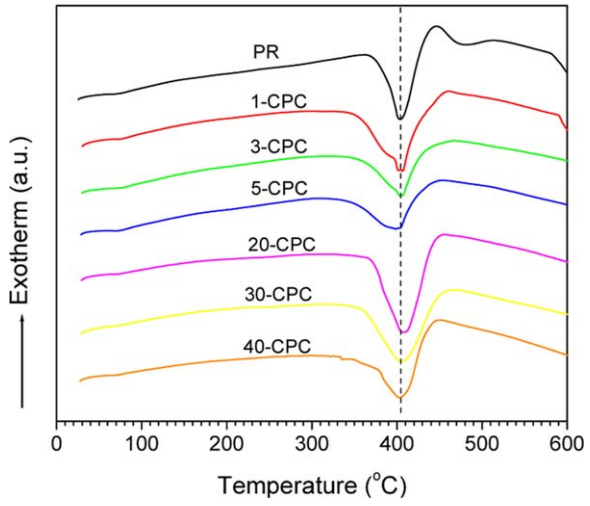

Figure 13. DTA thermograms of PR and CPC with 1, 3, 5, 20, 30, and 40 wt% CB contents. [Color figure can be viewed in the online issue, which is available at wileyonlinelibrary.com.]

TGA were performed to measure the amount and rate of changes in the mass of the samples as a function of temperature in a nitrogen atmosphere. Figure 14 illustrates the TGA thermograms of various samples. It seems that the weight loss starts nearly at 190°C and the loss pattern is apparently found to be different for different samples. Clearly, the weight loss delays by increasing the temperature with the increase of CB content. Two indicators commonly practiced to characterize the onset and structural degradation are the onset temperature (T_o) and

Table I. The T_d, T_o, T_{50}, and Residue Contents of Different Samples

Sample	wt%	T_d	T_o	T_{50}	Residue content at 600°C (wt%)
Pure PR	0	401	213.3	373.5	1.34
1-CPC	1	403	218.1	380.3	5.80
3-CPC	3	402	223.9	383.3	9.05
5-CPC	5	402	225.7	386.9	11.46
10-CPC	10	402	231.9	392.8	16.61
20-CPC	20	404	239.5	398.7	25.36
30-CPC	30	406	244.1	398.9	36.36
40-CPC	40	406	251.9	397.6	43.05
50-CPC	50	405	259.9	397.0	61.14

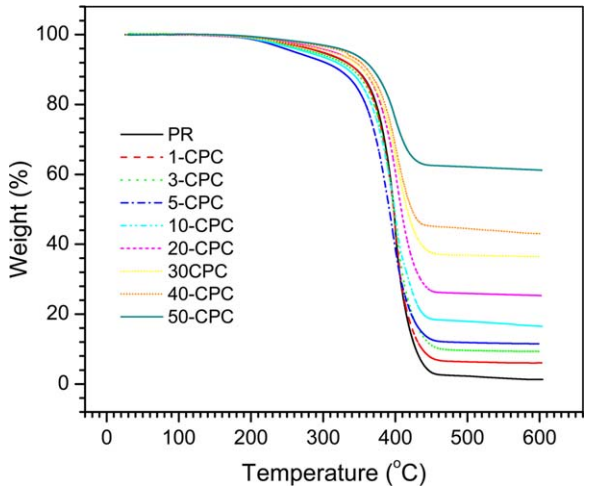

Figure 14. TGA curves of PR and CPC with 1, 3, 5, 10, 20, 30, 40, and 50 wt% CB contents. [Color figure can be viewed in the online issue, which is available at wileyonlinelibrary.com.]

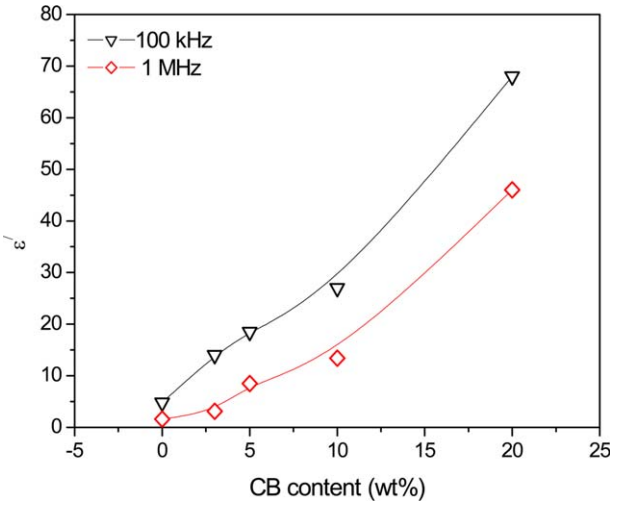

Figure 16. Comparison of dielectric constants at two different frequencies and different loading of CB particles. [Color figure can be viewed in the online issue, which is available at wileyonlinelibrary.com.]

destabilization temperature at 50% weight loss (T_{50}).[30] However, T_o, T_{50} and the residue content at 600°C have been analyzed and tabulated (Table I).

As the CB content is increased, the onset of decomposition is moved to higher temperatures. For instance, the T_o gradually increases from 213 for PR to 259°C for 50-CPC. On the other hand, T_{50} successively increases from 373 for PR to 396°C for 40-CPC. Thus, the thermal stability of the composites considerably increases. There are several chemical/physical mechanisms that could affect the stabilization effect of composites due to CB. These mechanisms include the reaction of free radicals coming from the resin matrix with CB, the adsorption of volatile degraded components on CB surface, barrier effect of CB and the reduction of molecular mobility of the resin molecules surroundings CB. The significant increase in T_{50} under inert atmosphere could be related to the barrier effect of CB which may decrease the diffusion of released oxygen from the resin into composites. Besides, adsorption of volatile components on CB surfaces may retard the degradation process. Therefore, the increase in interfacial area between resin and carbon black content up to 50 wt% enhances the thermal stability of composites considerably. From this TGA measurement, it can be noted that the thermal stability of the CPC is enhanced with the inclusion of CB content. Moreover, with the increase of the CB content agglomeration of CB particles occurs for which each resin molecule face large surface area of CB particles that encounter the segmental mobility of resin molecules. On the other hand, the residue content (wt%) at 600°C is increasing with the increase of the CB content. This is due to fact that for the high degradation temperature of graphite much greater than 600°C, the CB virtually remains as residue and not degraded at all.

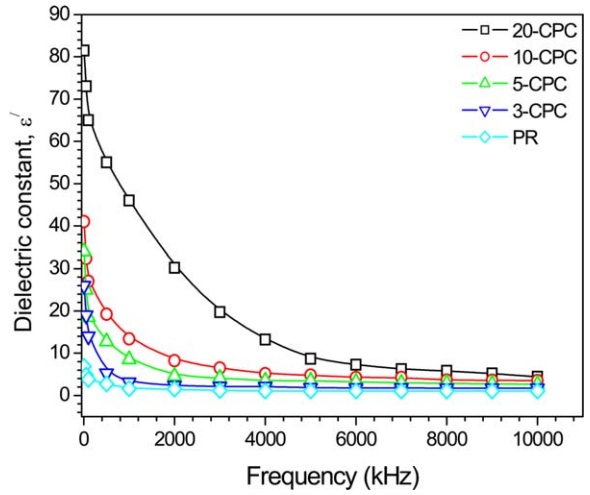

Figure 15. Dielectric constant versus frequency for various samples. [Color figure can be viewed in the online issue, which is available at wileyonlinelibrary.com.]

Electrical Properties

Figure 15 illustrates the ε versus frequency plots for various samples in the range of 1 kHz−10 MHz and Figure 16 shows the variation of ε with respect to CB contents at two different frequencies. For all samples, the value of ε is observed to decrease up to 5 MHz and after this, the decrease is very small. The observed decrease in the ε value seems to disobey the usual relaxation processes as described by the so-called Debye theory.[31] A larger difference in the ε values at lower frequency region than higher frequency region is observed in case of CPC, while this difference in case of PR is not conspicuous. This result suggests a development of frequency dependent ε value after CB loading, and the increasing CB content makes these differences larger. The CB is reportedly a semiconducting material and not dielectric by itself.[32] If CB is covered with insulator like PR, it may behave as a dielectric material by generating space charge polarization at the interfaces. According to Maxwell–Wagner–Sillar theory, the dielectric loss occurs due to the interfacial polarization of heterogeneous materials with conductive filler lower than the percolation threshold.[33] The interfacial polarization can easily occur with lower frequency due to the

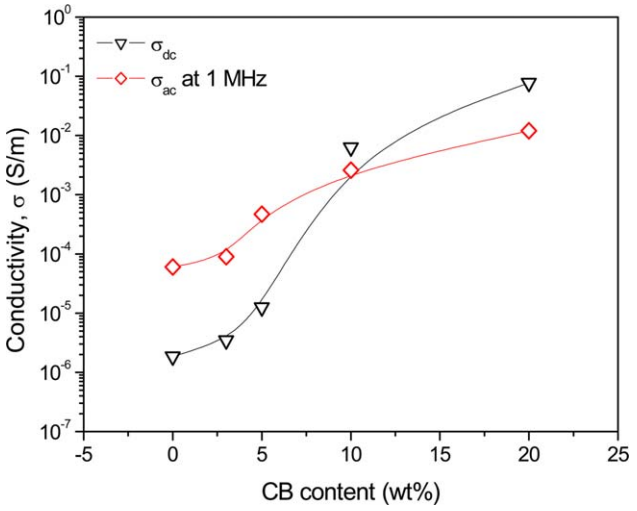

Figure 17. The change in DC and AC electrical conductivities with CB contents. [Color figure can be viewed in the online issue, which is available at wileyonlinelibrary.com.]

number of interfaces between CB and PR matrix. This polarization contributes to the improvement in dielectric properties of the composite filled with CB. At lower frequency the dipole is much responsive to the applied field, resulting in the higher ε value and as the frequency increases, the time required for interfacial charges to be polarized or the dipoles to respond the field variation is delayed, thereby contributing to the lower ε value.[34] Because of the increase of CB in PR, the amount of space charge polarization also increases, thus producing the higher ε value in CPC with higher CB content.

Figure 17 is plotted for the σ_{dc} and σ_{ac} variations with CB content. Both types of conductivities increase with the increase of CB content. The CPC shows conductivity due to dielectric loss, which increases with the increase of conductive filler. When the loading level of CB is below the level of percolation threshold, the conduction mechanism between the CB particles can primarily be explained by hopping and tunneling.[35] However, the difference in σ_{dc} and σ_{ac} values at a particular CB content are due to two different measurements techniques. The observed electrical properties of some of the resulting composites can be applied to the human phantom materials, as also suggested elsewhere.[32]

CONCLUSIONS

CPCs composites have been prepared by carbon black powder and liquid polyester resin with 0, 1, 3, 5, 10, 20, 40, and 50 wt% CB content and cured with 1% methyl ethyl ketone peroxide under a pressure of 50 MPa. FTIR spectra demonstrate the formation of physical bond, chemical bond like C—O—C and hydrogen bond. XRD shows a small crystalline part in PR matrix. The crystallinity of the samples increases and their average crystallite size decreases with the increase of CB content. SEM exhibits a good dispersion of particles in PR matrix at lower loading and inhomogeneous dispersion at higher loading. The tensile and flexural strengths of the composite decrease with the increase of fillers, and these decreases are explained on the basis of Nielson model. A significant increase in Young's and tangent modulii of about 80 and 100% is observed, respectively. A remarkable increase in microhardness of about 61% at 50 wt% CB content is also observed. This change in micromechanical property, such as microhardness, occurs due to the increased crystallinity in PR and more especially due to the inclusion of crystalline CB particles. TGA shows an increased thermal stability of the samples from 373°C for pure PR to 393°C for CPC. The dielectric constant of CPCs decreases with increasing frequency and increases with CB content up to 20 wt%, whereas the conductivities, σ_{dc} and σ_{ac}, of CPCs increases with increasing CB content. A model for physical crosslinking between PR and CB is proposed that supports both experimental and predicted results. The observed properties of the resulting composites can be useable in any suitable applications like indoor and outdoor panels, structures, bodies, furniture, phantom materials and commodities.

ACKNOWLEDGEMENT

The authors acknowledge the Bangladesh University of Engineering and Technology for financial support and Bangladesh Counsel of Scientific and Industrial Research for allowing all of this study. The authors express their thanks to Professor Md. Abu Hassan Bhuiyan for allowing electrical measurements.

REFERENCES

1. Psarras, G. C.; Manolakaki, E.; Tsangaris, G. M. *Compos. A* **2003**, *34*, 1187.
2. Bloor, D.; Donnelly, K.; Hands, P. J.; Laughlin, P.; Lussey, D. *J. Phys. D Appl. Phys.* **2005**, *38*, 2851.
3. El-Tantawy, F. *J. Appl. Polym. Sci.* **2005**, *98*, 2226.
4. Abdel-Aal, N.; El-Tantawy, F.; Al-Hajry, A.; Bououdina, M. *Polym. Compos.* **2008**, *29*, 804.
5. Yasmin, A.; Daniel, I. M. *Polymer* **2004**, *45*, 8221.
6. Genhua, Z.; Wu, J.; Wang, W.; Pan, C. *Carbon* **2004**, *42/14*, 2839.
7. Prasse, T.; Schulte, K.; Bauhffer, W. *Colloid. Surf. A* **2001**, *189*, 183.
8. Obayi, C. S.; Odukwe, A. O.; Obikwelu, D. O. N. *Nigerian J. Technol.* **2008**, *27*, 20.
9. Donnet, J. B.; Bansal, R. C.; Wang, M. J. Carbon Black: Science and Technology; CRC Press: Boca Raton, FL, **1993**.
10. Dhawan, S. K.; Singh, N.; Rodrigues, D. *Sci. Technol. Adv. Mater.* **2003**, *4*, 105.
11. Xie, S. H.; Zhum, B. K.; Xu, Z. H.; Xu, Y. Y. *Mater. Lett.* **2005**, *59*, 2403.
12. Zhao, Z.; Wu, W.; He, E.; Chen, Z. *Mater. Lett.* **2003**, *57*, 3082.
13. Novak, I.; Krupa, I.; Chodak, I. *Eur. Polym. J.* **2003**, *39*, 585.
14. El-Tantawy, F. *J. Polym. Sci.* **2005**, *97*, 1125.
15. Mamunya, Y. P.; Davydenko, V. V.; Pissis, P. *Eur. Polym. J.* **2002**, *38*, 1887.
16. Li, Y.; Wang, S.; Zhang, Y.; Zhang, Y. *J. Appl. Polym. Sci.* **2006**, *99*, 461.

17. Kurpa, I.; Novak, I.; Chodak, I. *Synth. Metals* **2004**, *145*, 245.
18. Han, G.; Lei, Y.; Wu, Q.; Kojima, Y.; Suzuki, S. *Polym. Environ.* **2008**, *16*, 123.
19. Zhou, D.; Cao, M.; Gong, S. *Mater. Sci. Eng. B* **2003**, *99*, 399.
20. Bhuiyan, M. K. H.; Rahman, M. M.; Mina, M. F.; Islam, M. R.; Gafur, M. A.; Begum, A. *Compos. A* **2013**, *52*, 70.
21. Chowdhury, F. U. Z.; Bhuiyan, A. *H.* **2000**, *370*, 78.
22. Dyre, J. C.; Schroder, T. B. *Rev. Mod. Phys.* **2000**, *72*, 873.
23. Cecen, V.; Seki, Y.; Sarikanat, M.; Tavman, I. H. *J. Appl. Polym. Sci.* **2008**, *108*, 2163.
24. O'Reilly, J. M.; Mosher, R. A. *Carbon* **1983**, *21*, 47.
25. Ungár, T.; Gubicza, J.; Ribárik, G.; Pantea, C. *Carbon* **2002**, *40*, 929.
26. Nielson, R. Mechanical Properties of Polymers and Composites; Marcel Dekker: New York, **1974**.
27. Flores, A.; Ania, F.; Balta Calleja, F. J. *Polymer* **2009**, *50*, 729.
28. Balta Calleja, F. J.; Fakirov, S. Microhardness of Polymers; Cambridge University Press, UK, **2000**.
29. Fu, S. Y.; Feng, X. Q.; Lauke, B.; Mai, Y. W. *Compos. B Eng.* **2008**, *39*, 933.
30. Mina, M. F.; Seema, S.; Matin, R.; Rahman, M. J.; Sarker, R. B.; Gafur, M. A.; Bhuiyan, M. A. H. *Polym. Degrad. Stab.* **2009**, *94*, 183.
31. Dekker, A. J. Solid State Physics; Macmillan India Ltd: India, **1981**; Chapter 6.
32. Moon, K. S.; Choi, H. D.; Lee, A. K.; Cho, K. Y.; Yoon, H. G.; Suh, K. S. *J. Appl. Polym. Sci.* **2009**, *77*, 1294.
33. Chung, K. T.; Sabo, A.; Pica, A. *J. Appl. Phys.* **1982**, *53*, 6867.
34. Paul, A.; Thomas, S. A. *J. Appl. Polym. Sci.* **1997**, *63*, 247.
35. Ku, C. C.; Liepins, R. Electrical Properties of Polymer; Hanser Publishers: Munich, **1987**; p 334.